IEEE Journal of Microwaves

Received 18 August 2022; revised 21 October 2022; accepted 16 November 2022. Date of publication 13 December 2022; date of current version 6 January 2023.

Digital Object Identifier 10.1109/JMW.2022.3224087

A Flexible Tuned Radio-Frequency Planar Resonant Loop for Noninvasive Hydration Sensing

SEN BING (Graduate Student Member, IEEE), KHENGDAULIU CHAWANG (Student Member, IEEE), AND J.-C. CHIAO (Fellow, IEEE)

(Regular Paper)

Electrical and Computer Engineering, Southern Methodist University, Dallas, TX 75205 USA

CORRESPONDING AUTHOR: Sen Bing (e-mail: sbing@smu.edu).

This work was supported by the National Science Foundation under Grant ENG-CMMI-1929953, and in part by the Mary and Richard Templeton endowment. This work involved human subjects or animals in its research. Approval of all ethical and experimental procedures and protocols was granted by Southern Methodist University IRB committee (protocol ID: H21-023-CHIJ).

ABSTRACT In this work, a planar radio-frequency sensor based on a flexible polyimide substrate has been developed to monitor the water content changes noninvasively and efficiently in a human body or tissues. The sensor is based on the detection of electromagnetic resonance that is susceptible to dielectric property changes by water content variations. The planar loop resonator tuned with a metal pad features improved resonance, compact size, and flexibility to conform to a curved surface. Designs and experiments to continuously monitor human hydration processes *in vivo* have been demonstrated. The recorded data shows distinct trends when a person becomes hydrated from a dehydrated state. Discrete and continuous measurements are compared with the simulations conducted by using documented, generalized human skin permittivity properties. Discrepancies between the measurements and simulations are investigated and verified with directly measured skin permittivities. Measurements variations are also investigated. With the advantages of being compact, flexible, and planar, the sensor can be integrated into a wearable on the human forearm. Additionally, the sensor has been used to demonstrate its ability to detect water content changes in a phantom made of ground pork. The *ex vivo* results indicate the sensitivity and consequential variations in practical scenarios. The promising results show great potential for human body monitoring and also general applications in agriculture and the food processing industry from the demonstration of the sensing principle in the pork phantom.

INDEX TERMS MTT 70th Anniversary Special Issue, hydration, non-invasive, planar resonant sensors, loop resonator, impedance matching, water sensing.

I. INTRODUCTION

Dehydration is a condition of lacking adequate water in the body. In general, more than 2% of body water loss can cause dehydration symptoms [1], leading to severe or even deadly health problems. For example, in a dehydrated state, the heart is forced to beat faster to compensate for the decrease in body blood circulation [2], potentially causing cardiovascular strain and damage to the heart and arteries [3], [4]. A well-hydrated state reduces the risk of heart failure, according to [5]. Dehydration also decreases the capacity to generate upper and lower body anaerobic muscular power, leading to a higher risk of musculoskeletal damage [6], [7], including muscle cramping and fatigue, which frequently occurs in marathons and triathlons [8], [9]. It has been well documented that dehydration can cause acute or chronic kidney injuries [10], [11], [12], [13], [14], [15], particularly they are important for certain groups of workers in the fields [16], [17] and urinary tract infections [18], [19], [20]. Seizures are also related to dehydration in patients with epilepsy and children [21], [22], [23], [24]. Apart from the physiological stress, dehydration

also affects mental functions such as cognitive performance and mood [25] mainly due to shrunk blood vessels in the brain, and inefficient fluid supply [26]. Without normal water homeostasis, chronic neuronal dysfunction can lead to multiple neurodegenerative diseases, including dementia [27]. Therefore, maintaining a well-hydrated state is vitally important for body health.

The feedback mechanisms for a healthy person included in the urinary system and the sensation of thirst mainly regulate the balance of hydration by adjusting the urine volume [28] and intake volume of fluid inspired by the thirst feeling [29]. However, evaluating dehydration is challenging for people with diminished feedback mechanisms, including infants [30], [31], the elderly people [32], outdoor worker, athletes, and soldiers who are very concentrated on their tasks. Monitoring hydration levels becomes exceptionally vital for those people with a higher risk of dehydration. If detected early, severe situations or long-lasting consequences can be avoided as minor dehydration can be treated simply by fluid intake [33].

To access the feasibility of hydration level detection, a series of dehydration measurements have been conducted, which were based on detecting the variations in dielectric properties of measured tissues, largely determined by the water content of biological tissues with radio frequency (RF) and microwave signals [34], [35], [36]. Shahzad et al. [37] conducted *ex vivo* dielectric dehydration measurements using an open-ended coaxial probe from 500 MHz −20 GHz on the freshly excised rat liver samples. The dielectric parameters were recorded at different time points post-excision, and the measurements showed decreasing shifts of more than 25% in both the real and imaginary parts of complex permittivity during 3.5 hours after excision. Pollacco et al. [38] investigated the correlation between the dielectric properties of biological tissues and different hydration levels from the measurements conducted on rat muscle and fat tissues *in vivo* and *ex vivo*. Dielectric parameters were measured from 500 MHz to 50 GHz at the constant room temperature of 77 °F, showing the muscle tissue with a higher percentage of water content, compared to the fat tissue, represented a higher dielectric constant and conductivity. Similar trends can be found and verified in literatures with different means of measurements [39], [40], [41], [42], indicating that the dielectric properties of biological tissues are mainly affected by water contents. It can be explained because of the high dielectric constant of water and the presence of free ions from water in tissues, which increase conductivity. As a result, dehydration thus leads to a decrease in dielectric properties. Based on this correlation, RF and microwave sensors have been designed and used for water content sensing [43] with three major principles: resonance, transmission, and reflection.

Resonance cavities can acquire frequency characteristics from interferences in the media, and dielectric properties of the media can be calculated from the spectral characteristics, typically assuming the media are homogenous and isotropic or with simple layer configurations if not homogenous. However, measurements using conventional resonance cavities are limited for targeted media with high dielectric losses [44]. The physical shapes of conventional high-Q (quality factor) cavity resonators [45], [46], [47] are constrained to be used on the human body as a wearable sensor for continuously monitoring. Split ring resonators have been used for probing tissue properties for the features of being planar and with higher sensitivities compared to the conventional loop resonators. Two split rings in a cavity placed on a person's abdomen to monitor blood glucose levels have been demonstrated with clinical evidence [48], [49]. One split ring closer to the skin detected the tissue changes while the other ring served to provide the reference frequency. Relative frequency shifts gave insights into blood glucose variations. The cavity was fairly large, so it was not convenient to wear for a long time. A planar split ring between a transmission line made on a rigid composite substrate (ROGERS 5880 PTFE) was used to monitor blood glucose [50]. The demonstration was performed on dead skin samples with controlled interstitial fluid mimicking different scenarios in tissues showing clear frequency shifts. However, the quality factor of the resonator was not mentioned. Similarly, a large array of split rings coupled to a transmission line on a rigid substrates (ROGERS Duroid 6010) was made to evaluate dielectric properties on multiple points of a dead tissue sample [51]. A complementary split-ring was also proposed for sensing tissue types and demonstrated with dead animal tissue samples [52].

The transmission methods consist of transmitter and receiver antennas, by which electromagnetic fields go through and interact with the measured media. Garrett et al. designed a transmission sensor to measure human hydration levels. With the electromagnetic waves passing the forearm, the effective permittivity could be mathematically evaluated and classified into hydrated or dehydrated state groups [53], [54]. Later, the method was utilized to conduct human experiments on fasting participants [55]. However, such a system might be bulky, and this had a lower potential for wearable purposes. It was difficult for long-term continuous monitoring due to discomfort unless the antennas can be made planar with conformability. Under such constraints, participants in the transmission measurement were only recorded before and after excise in discrete time points, by which other metabolism activities may raise the possibility of error in calculations. Besides, high field density may raise safety concerns as the transmitted powers, especially in local areas, may not be controlled well for different body types.

The reflection method has relatively simpler physical structures, which can be potentially designed as a wearable for long-term continuous monitoring. The inducing electromagnetic wave interacts with the measured media, and the reflection coefficient can be evaluated to distinguish the dielectric properties of the media. Typically, the reflection sensor requires a dynamic matching circuit to achieve better resonance performance for its transmission and reflection modes. The matching circuits are usually bulky and bring design constraints. Additionally, near-field characteristics, sizes, and wave scattering across different layers of tissues in reflection

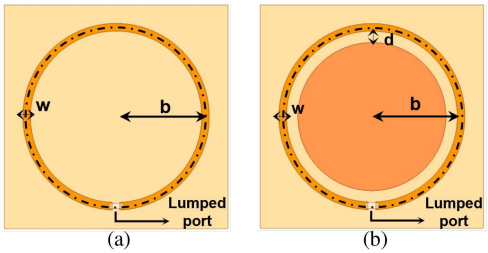

FIGURE 1. (a) Loop resonator configuration: the radius $b = 11.75$ mm; the loop width $w = 1$ mm; and the tuning gap d between the pad and loop. (b) Loop resonator with a tuning center pad. The tuning gap $d = 1.5$ mm, between the pad and loop.

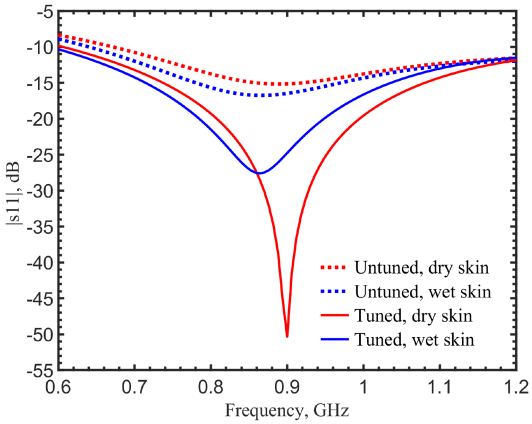

FIGURE 2. Simulations of the reflection coefficients conducted with documented human skin properties [63] with (tuned) and without the center pad (untuned), compared to measurements.

coefficient measurements make it challenging to design planar antennas with compact sizes as wearables to accomplish the required reliability and stability for different body types. Brendtke et al. [56] proposed a broad-band antenna at 7.9 GHz to measure the reflection coefficient on the skin equivalents that were made of cells and hydrogel with specific hydration and density of matrix components. Results indicated resonant frequencies and return losses were related to the corresponding skin equivalents and could be evaluated to determine hydration level provided by the designed skin equivalent. Kilpijärvi et al. [57] designed a reflection sensor based on a complementary split-ring resonator (CSRR) pattern. The sensor is fabricated on an SMA connector that connected to a vector network analyzer (VNA), behaving as a dielectric probe. A series of different combinations of carbon black powders and barium strontium titannate were used with urethane rubber as skin phantoms to mimic the dielectric properties of dehydrated skins. The SMA connector formed a feeding structure to the CSRR. So the sensor may not be suitable for applications that require a planar and deformable configuration.

This work developed a flexible near-field planar resonant loop as a wearable for non-invasive water monitoring, in addressing the aforementioned constraints in different types of measurements methods and demonstrating *in vivo* on the human body. The design is based on a planar loop [58], as shown in Fig. 1(a), with a metal pad embedded, as shown in Fig. 1(b). The planar loops in Fig. 1(a) have been used widely for power coupling and sensing by static or RF magnetic fields. They provide simplicity and predictable characteristics in the air [58]. However, they have been limited by lower quality factors for resonance. The magnetic field sensing mainly depends on permeability instead of permittivity, to which the water content sensing effects are sensitive. The metal pad provides distributed capacitance [59] and mutual inductance [60] between the gap of the loop and the center pad in Fig. 1(b). The distance of this gap serves to tune the distributed capacitance and sequentially the mutual inductance to match the impedance of the loop at the desired resonant frequency. Thus, the sensitivity to resonance is influenced by the permittivity in the near-field region. The 900-MHz ISM (Industrial, Scientific, and Medical) band is chosen for the demonstration in this work. However, the principle can be applied for any frequency band. Similar designs with the same impedance matching concept have been investigated in our previous work to improve the power-transfer performance in subcutaneous implants [61], [62]. The results showed that the planar tuned loop can be designed to a compact size with excellent performance in resonance. Both are essential features for an effective wearable device. Measurements and simulations were conducted to investigate the feasibility of monitoring human hydration levels. Moreover, general water content monitoring experiments were conducted with a phantom made of ground pork to show potential sensor applications.

II. SENSOR DESIGNS

A. IMPROVEMENT OF RESONANCE AND SENSITIVITY

The proposed sensor was designed, shown in Fig. 1(b), to conform onto the forearm skin and operate at around 900 MHz. The loop radius was $b = 11.75$ mm with a metal width $w = 1$ mm. The gap between the loop and the center pad was $d = 1.5$ mm, which was optimized for the resonance on the human skin in the dehydrated condition. Considering the curvature of the forearm for a wearable, the tuned loop was fabricated on a flexible polyimide film (DuPont Pyralux FR9220R) that can be firmly in contact with the skin. The copper pattern was etched after photolithography was applied with a photomask on the photoresist-covered film. A previous demonstration of the tuned loop for a wirelessly-powered implant application was conducted on rigid substrates [61]. The thickness of the film is 76 μm with a dielectric constant of 3.2. The copper thickness on the film is 70 μm. Finite-element simulations for the loop resonators with and without the tuning pad, on dry (dehydrated) and wet (dehydrated) skins, were conducted for comparison. The human skin dielectric properties were obtained from the documented library in [63]. It should be aware that this database does not define a quantitative level of hydration for dry or wet skins and is highly generalized, so discrepancies with measurements on individuals are expected.

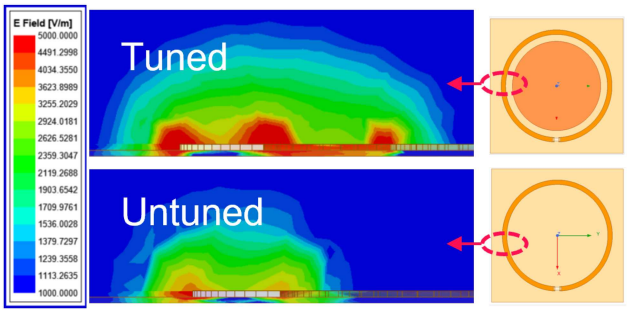

FIGURE 3. Comparison of electric fields for the loop resonator with or without the tuning pad.

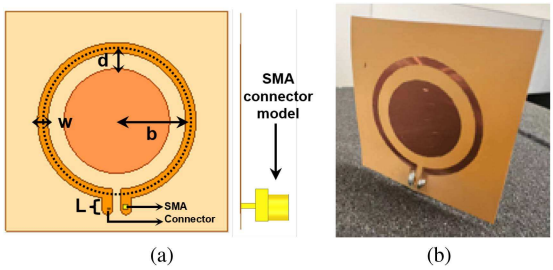

FIGURE 4. (a) The architecture of the connection-improved sensor: the radius $b = 14.3$ mm, loop width $w = 2$ mm, leg length $L = 3$ mm, tuning gap $d = 3.1$ mm. (b) Photograph of the sensor connected with an SMA connector.

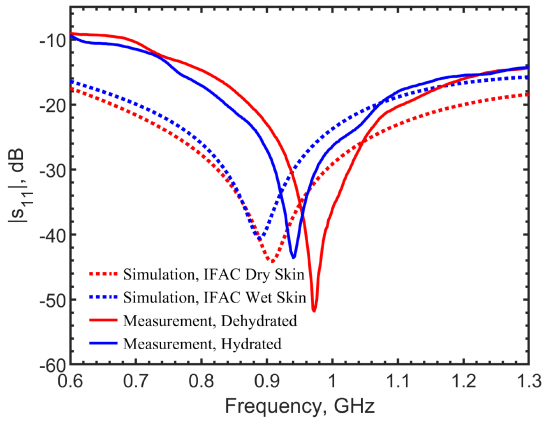

FIGURE 5. Comparisons of simulation results utilizing human dry and wet skin properties documented in the IFAC library [63], and measurements on the forearm when participant was dehydrated or hydrated.

Fig. 2 shows the comparison of reflection coefficients. For dry skin, the single loop (red dash curve) has a resonant frequency at about 888 MHz with $|s_{11}|$ of -15.17 dB, whereas the sensor with the center pad (solid red curve) has a resonant frequency of 900 MHz with $|s_{11}|$ of -50.33 dB. The spectral shapes clearly indicate a significant enhancement in resonance with the $|s_{11}|$ improved by 35 dB. With the wet skin model, the loop experienced a frequency shift of 2%, while it was 4% for the tuned loop, as shown clearly in Fig. 2, from 900 to 864 MHz. The shift was distinct due to the better resonance that induced electric fields deeper into the tissues. Fig. 3 shows the higher intensity of electric fields in the tuned loop case, thus, the effective dielectric constant changes became more pronounced to affect the resonance.

B. MEASUREMENTS

The inside of the forearm is selected for sensing. The skin is relatively thin for electric-field probing. The forearm area has close vicinity to the artery that delivers blood from the heart, it receives water from the bloodstream quicker than other body parts. The forearm provides access for a convenient and comfortable wearable. The sensor was placed on a person's forearm with medical-grade tapes (3M Nexcare Durapore Durable Cloth Tape, USA) fixed to avoid movement. A 50-Ω SMA adaptor connected the resonator to a vector network analyzer (Keysight PNA N5227B). However, during the measurements, the connectors and soldering parts made the person feel uncomfortable and made it challenging to maintain firm contact with the skin. The horizontal connection from the leg and center conductor of the SMA connector experienced a contact issue between the substrate and the skin. Due to the mechanical tension from the rigid coaxial cable, coupled with the high sensitivity in resonance, measurements showed noticeable variations when applying different pressures on the connector. Similar phenomena in which probe contact pressures affected the RF measurements on tissues were observed [64]. To solve this issue, an improved sensor has been built.

The sensor was modified with two vias to mount the SMA adaptor vertically from the backside of the substrate. This allowed the sensor surface fully and firmly in contact with the skin. The contact between the SMA and the vias was not affected by the cable tension. Furthermore, the vertical cable arrangement permitted the cable to be mechanically supported by an elevated surface to ease tension. The loop was redesigned with a radius $b = 14.3$ mm with a leg length $L = 3$ mm. The spacing d between the loop and tuning pad was tuned at 3.1 mm. Fig. 4 shows its dimensions and a photo of the tuned loop on a flexible polyimide substrate.

Simulations with the documented dry and wet skin permittivities [63] were conducted, and the results are shown in Fig. 5. The sensor was tuned for the dry skin condition to operate at 906 MHz with a $|s_{11}|$ of -45 dB. The resonant frequency should shift to 888 MHz for the wet skin. Compared to simulations, the measured hydrated (wet) skin had a resonant frequency at 940 MHz while it was at 972 MHZ for the dehydrated (dry) skin. The creation of hydrated and dehydrated conditions in a person is discussed in a later section. The discrepancy in the resonant frequencies between the theoretical dry skin and the dehydrated person was 66 MHz. The discrepancy is 52 MHz for the theoretical wet skin and the hydrated person. The mismatch was due to the generalization of skin permittivities in the documented library used in simulations and that measurements for the individuals depended on the actual dehydrated levels at the time of the experiment.

To verify the source of mismatch, dielectric properties measurements on the human forearm were conducted using

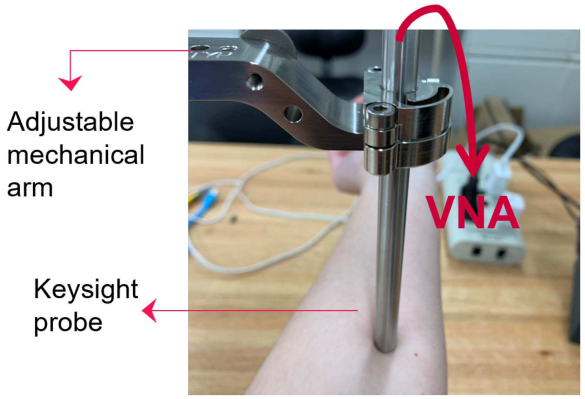

FIGURE 6. Setup of skin dielectric properties measurement using the dielectric constant probe kit.

a coaxial probe kit (Keysight N1501 A). When the person was in the dehydrated or fully hydrated states, the probe was placed on the skin of the forearm, as shown in Fig. 6, and multiple dielectric properties measurements were repeated in the same location. The person stopped liquid and food intake after dinner and jogged for 45 minutes in the morning. After sweat was wiped and heart rate/body temperature returned to those before jogging, the probe was placed to measure the dielectric property of skin in the dehydrated state. Then the person started drinking water slowly and continuously for 30 minutes. After 30 minutes, if the reflection coefficients stayed unchanged, it was considered in a fully hydrated state. The measured dielectric constants (solid curves) are shown in Fig. 7(a), compared to those from the documented dataset [63]. The error bars show the ranges in 4 measurements. It was observed that pressure on the skins affected the measurement results, so the probe was pushed lightly on the skin, and multiple measurements were taken quickly. There were noticeable discrepancies in the skin dielectric properties between the generalized library dataset and the measurement from the individual person. This is expected because the datasets are generalized cases. The dehydrated (dry skin) levels also depended on individuals' physiological conditions. Using the measured dielectric constants in the models, Fig. 7(b) shows the simulations of reflection coefficients for the tuned loop resonator compared to those using the documented library dataset. The discrepancy between using the measured skin data from a dehydrated individual and using the generalized skin data was 67 MHz. The discrepancy was 55 MHz for wet/hydrated conditions. Fig. 7(a) and Fig. 7(b) highlight the mismatch between the generalized skin dielectric constants and the measured ones, as well as the effect on resonance. Thus, we further considered including both the permittivity and conductivity of the dehydrated and fully hydrated tissues measured from human bodies in simulation. Fig. 8(a) shows the measured dielectric constants and loss tangents from 600 MHz to 2 GHz in one individual person. It should be noted that even with the same person, whose dehydrated and hydrated states should be the same, the measurements still contained deviations, as shown by the error

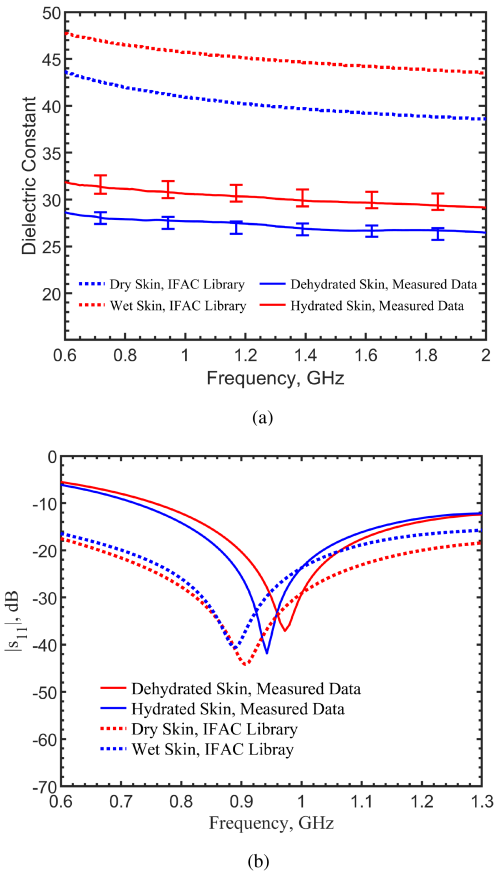

FIGURE 7. (a) Comparisons of dielectric constants measured with the probe, compared to the IFAC library dataset [63]. The error bars in the measured results were obtained from 4 measurements. (b) Simulations of the reflection coefficients in the tuned loop sensor by using the IFAC documented human skin and by the measured dielectric constants on the skin with the probe.

bars in Fig. 8(a). Utilizing the measured parameters in simulations, the resonant frequency for the dry skin was 972.5 MHz and shifted to 942.5 MHz for the wet skin. During the measurements for dielectric constants and loss tangents, our tuned loop resonator was also placed on the forearm near the probe, and the resonant frequencies were measured at 972 MHz and 940 MHz, respectively, for the dehydrated and fully hydrated states. The simulations and measurements match well, as shown in Fig. 8(b). The resonance performances were robust for both the dry and wet skin conditions, with their reflection coefficients better than −37 dB.

III. CONTINUOUS HYDRATION MONITORING FOR HUMAN BODY

A. EXPERIMENT SETUP

The sensor was conformed onto the skin of the left forearm and connected to a vector network analyzer (Keysight PNA N5227B). Considering different sizes in persons, a fixed measurement point became difficult. We conducted the measurements approximately 5 cm to the wrist on the forearm. Due to the high sensitivity of the tuned sensor and the mechanical tension from the coaxial cable, a small movement

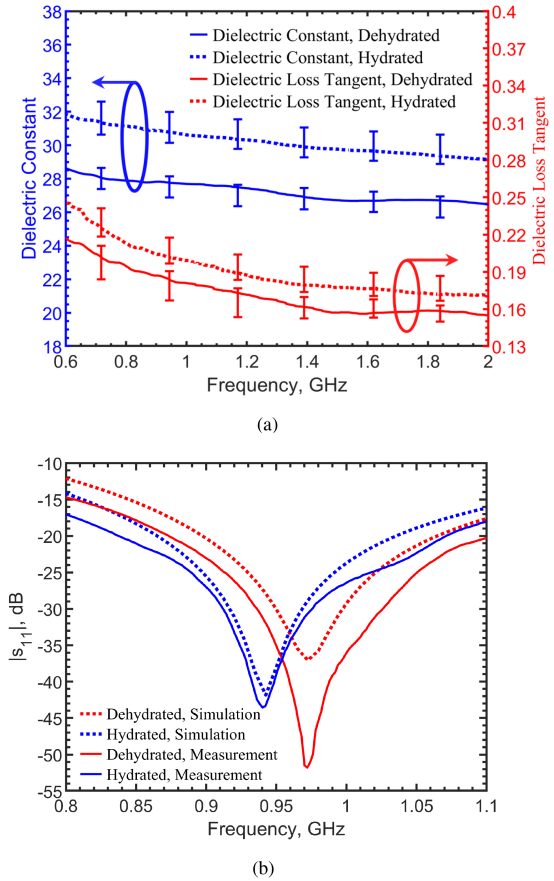

FIGURE 8. **(a) Measurements of dielectric properties for dehydrated and hydrated human skins. The error bars were obtained from 4 measurements at the same location on the forearm. (b) Simulated reflection coefficients for the tuned resonator utilizing the measured human skin dielectric properties, compared to measured results by the tuned loop.**

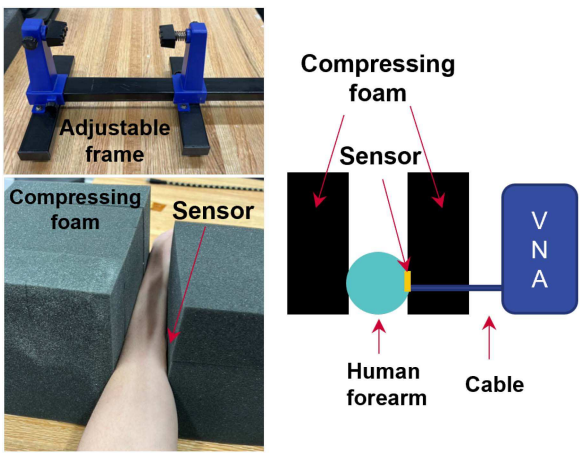

FIGURE 9. **Setup of the human hydration monitoring measurements.**

of the forearm caused measurement fluctuation, even with the vertically-mounted SMA adaptor. To further improve the stability, comfort was also important during the experiment since muscle fatigue occurrence was observed during experiments, and it induced involuntary motion of the arm. Fig. 9 shows the setup. An adjustable frame and elastic porous foams pressed the sensor firmly on the forearm. The compressing foam ensured by the adjustable frame comfortably conformed the sensor on the skin without feeling noticeable forces. The person could sit with the arm relaxed on the table during the long measurement period.

The experiments were designed to demonstrate the capability of continuously monitoring a person's hydration level *in vivo*. As it was difficult to create real-time and controlled scenarios of different human dehydration levels or have a means to independently and quantitatively verify the dehydration levels, the experiments aimed to investigate the measurements during the hydration process from a dehydrated state. The subject stopped the water, liquid, or food intake after 10 PM on the night before experiment. At 9 AM the next day, the subject jogged for 45 minutes on a treadmill to induce sweating. After wiping out sweat, the subject rested until the skin became dry, heartbeat rates, and body temperature went back to normal. It was assumed that the subject was in a dehydrated state, verified by verbal acknowledgment of the person about feeling thirsty, although the dehydration level was not controllable or quantifiable because of variations in physiological conditions of individuals at different times. The human subjects research protocol ID is H21-023-CHIJ, approved on April 19, 2021, by the Southern Methodist University IRB committee. Reflection coefficients were automatically recorded by the VNA every 20 seconds as soon as the subject started to sip water slowly and continuously while sitting without moving until 1000 mL of water was consumed. A program in MATLAB codes automatically sorted out resonance points in the frequency range of 0.1−2 GHz. It was found that the resonant frequencies in all cases plateaued within 25 minutes of hydration. The recorded resonant frequency at the fully hydrated state was used as the baseline, and frequency shifts in percentage were calculated for other resonant frequencies. A moving average of 10 samples was applied to all data to illustrate the trends.

B. RESULTS AND ANALYSIS

Fig. 10 shows the results of five cases. The initial dehydrated levels had frequency shifts from the baseline in percentage of 1.1%−2.5%, which depended on the individual physiological conditions. It was expected that it took more time to reach the fully hydrated state from a more serious dehydrated condition. The shaded area in Fig. 10 indicates the possible resonant frequency shift range. The gradual and monotonical trends showed clear evidence that the resonant frequency could indicate the body hydration level. The resonant frequency shifts changed faster in the first few minutes as the water entered blood vessels, which immediately altered the permittivities in the area electric fields reached. Simulations in later discussion showed the fields reached the dermis and hypodermis layers in the skin, which contain blood vassals and sweat glands. The trends gradually slowed down after a period of time. It might indicate that the water started entering cells until they were fully hydrated.

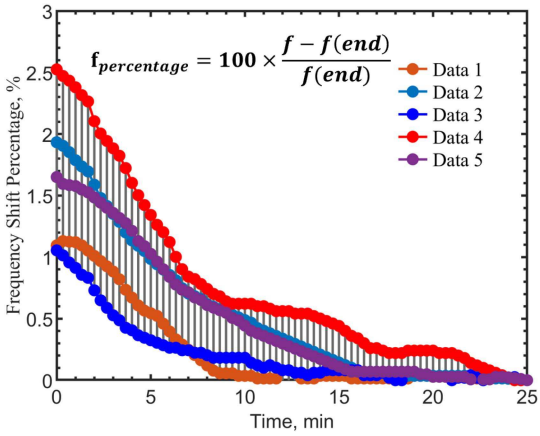

FIGURE 10. Resonant frequency shift in time during the human hydration for five dehydrated subjects. Resonance frequency was tracked along with reflection coefficient at an interval of 20 seconds continuously.

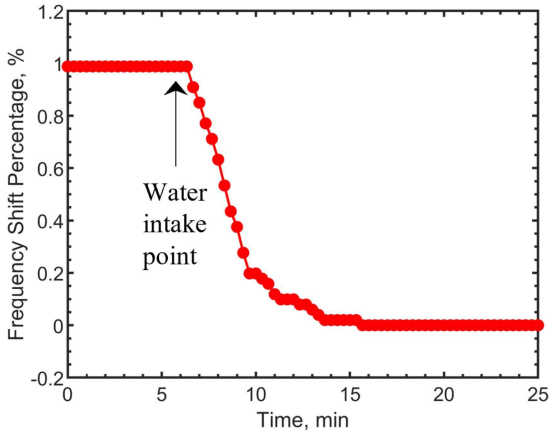

FIGURE 11. Resonant frequency shift in time during the human hydration experiment. The data recording began before the dehydrated participant's intake of water (50 ml volume).

Another experiment for hydration monitoring was conducted. The experiment followed the same protocol except that the subject only drank 50 mL of water in the beginning, instead of a total of 1000 mL continuously. The recording began prior to the time point when the subject started drinking water. The baseline resonant frequency was the one after 25 minutes. Fig. 11 shows the resonant frequency shifts calculated from the baseline. The results revealed a monotonical descending trend after 50-mL water intake. The flat curve before the water intake indicated the measurement stability and that the resonant frequency shifts were solely caused by the hydration level changes. The total frequency shift was 1%, which was much lower than the average frequency shift in the other fully hydrated cases, indicating the subject was in a partial hydrated status by only taking 50 mL of water. The results verified the feasibility of using the tuned resonator with a robust resonance for continuously and noninvasively monitoring hydrating and dehydration levels in the human body.

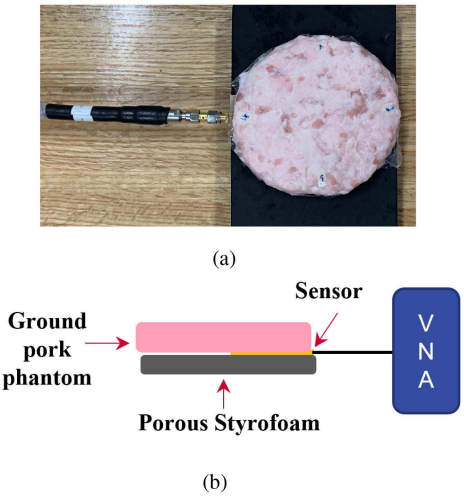

FIGURE 12. (a) Photo of the ground pork phantom used in the experiment. (b) Setup of the long-term water content monitoring experiments.

IV. INVESTIGATION WITH A PHANTOM MODEL

A. A PHANTOM TO INVESTIGATE WATER CONTENT

Specific hydration/dehydration conditions are difficult to create with good repeatability and control. We have created a phantom with moist ground pork for the intention to provide quantitative controls in experiments. The shape, thickness, weight, and added water volume were quantified to ensure experimental consistency. Proper amounts of water were mixed with ground pork to vary the water contents without water leaking to the bottom of the phantom. A 3D-printed cylinder disk with a height of 15 mm and a radius of 90 mm was used to pack ground pork. Fatty ground pork was chosen for its ability to better mix with water. Added water volume was 23 mL. After the ground pork was packed, it was removed from the disk and wrapped with a layer of plastic wrap. The phantom had the top surface exposed to air allowing water to evaporate, mimicking dehydration, as shown in Fig. 12(a). The proteins, however, on the surface gradually became solidified when exposed to air for a long time, slowing down water evaporation. The weight of the ground pork phantom was 91 g.

B. EXPERIMENTS

Fig. 12(b) shows the setup for long-term water content monitoring. The tuned loop resonator was placed underneath the ground pork phantom. Porous Styrofoam was used to support the phantom and sensor while alleviating the cable tension. Reflection coefficients were recorded every minute for 19 hours. The resonant frequency at the beginning of the experiment was used as the baseline, and frequency shifts in percentage were calculated at other time points. The experiments were repeated with five phantoms under the same protocol. The weights of the phantoms were recorded at the end of the experiment, shown in Table. 1. The weight loss percentages were treated as the water loss by evaporation.

Fig. 13 shows the measured resonant frequency shifts in time during the 19-hour experiments. All five datasets showed

TABLE 1. Weight Records of Moist Ground Pork Phantom

No.	Start Weight, g	End Weight, g	Weight loss, %	Frequency shift, %
1	91	80	12.09	8.26
2	91	82	9.89	6.17
3	92	81	11.96	10.27
4	91	79	13.19	13.39
5	91	81	10.99	7.92

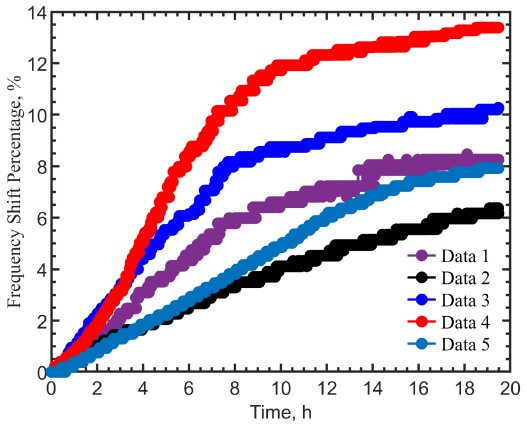

FIGURE 13. Resonant frequency shift as a function of time during the dehydration experiments using the ground pork phantoms.

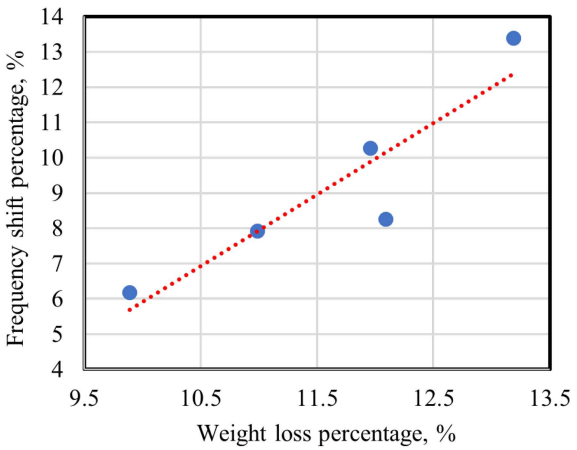

FIGURE 14. Total frequency shift in percentage as a function of the weight loss in percentage in the phantom after 19 hours of water evaporation.

the continuously and monotonically increasing trends of resonant frequencies from the baseline during water evaporation. The trends slowed down during the second half of the experiments, mainly because the top part of the water in the phantom has evaporated, and the top surface became hardened, reducing evaporation rates.

The total frequency shifts were 8.26%, 6.17%, 10.27%, 13.39%, and 7.92% from the baseline for the five experiments, shown in Table. 1, while the weight losses in percentage were 12.09%, 9.89%, 11.96%, 13.19%, and 10.99%, respectively. Fig. 14 shows the relationship between the frequency shift

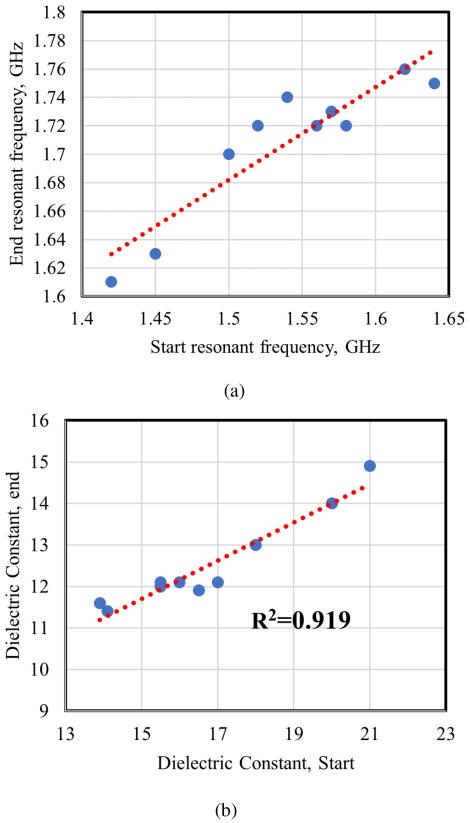

FIGURE 15. The start and end (a) resonant frequencies with their respective (b) effective dielectric constants calculated. The relationship with a linear regression $R^2 = 0.919$ showed how the effective dielectric constant changed with the water losses.

and the total water loss. It indicated more water losses led to more resonant frequency shifts, as expected. However, there was an inconsistency when comparing datasets 1 and 3. The water loss percentage in weight in dataset 1 was 12.09 %, with a smaller frequency shift of 8.26%, compared to the water loss of 11.96% with a frequency shift of 10.27% in dataset 3. It was hypothesized that this exception occurred because the ground pork phantom was not made uniformly across all areas with added water, and the resonator interacted with the tissues locally owing to confined field distributions. The localized resonance measurement then had a mismatch with the total weight change due to water evaporation.

To validates the hypothesis, the same experimental protocol was applied for ten measurements. Although the ground pork was mixed in a similar way and with the same weight and water amount, the resonant frequency at the start points of the experiments was different. The start and end resonant frequencies were recorded for each 19-hour experiment, as shown in Fig. 15(a). A correlation was found between the start and end resonant frequencies after the water evaporation. Simulations were conducted in a model where the tuned loop resonator was placed on the boundary of air and a medium. The medium was assumed infinite in dimensions with a dielectric constant varied from 5 to 60. Fig. 16 shows the resonant frequency

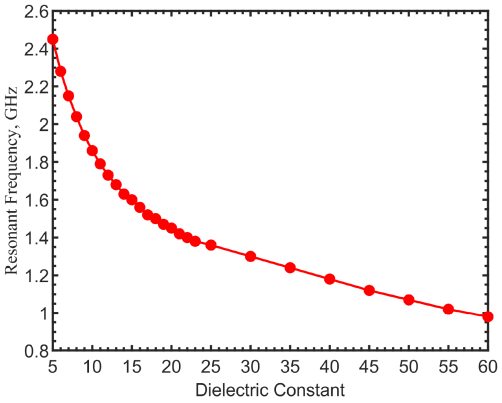

FIGURE 16. Simulations of resonant frequencies for the phantom in a range of dielectric constants varied from 5 to 60 due to water content changes.

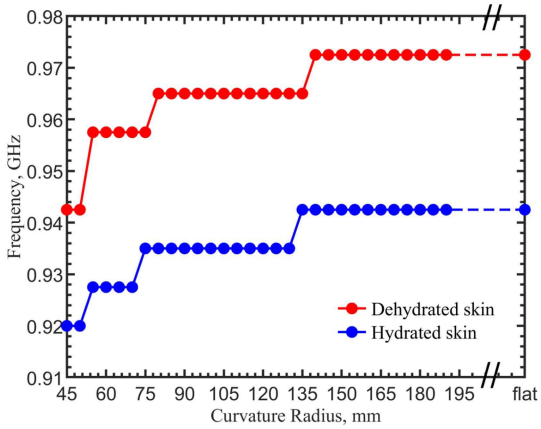

FIGURE 17. Simulations of the resonant frequency for models with different curvature radii. The model permittivities of dehydrated and hydrated states were measured by a dielectric probe on a human body.

as a function of the dielectric constant. The effective permittivity changes, induced by the water content changes, then could be calculated from the resonant frequencies, as shown in Fig. 15(b). The relationship with a linear regression $R^2 = 0.919$ showed how the effective dielectric constant changed with the water losses. Even though the start resonant frequency was different due to local tissues, its changes and associated dielectric constant changes from the water losses followed the same trend. The dielectric constants calculated from the resonant frequencies are the mixtures of ground pork and added water, before and after evaporation. The permittivities of dielectric mixtures can be approximated by the two-phase Wiener mixing formula [65], [66]. With the dielectric constants 5.9 [67], [68], [69] and 80 of blood-infiltrated fat and water, the start and end dielectric constants were used to calculate the mixture ratios. As fat tissues induced weak depolarization fields by the external fields, if a depolarization factor of 0.333 was assumed for spherical distributions of induced charges, comparing the permittivities before and after evaporation, the ratios of water loss in total mixture volumes were between 10% and 15% for the cases in Fig. 15(b).

V. DISCUSSION

A. SENSITIVITY ON FOREARM CURVATURES

The sensor was designed and fabricated on a flexible polyimide substrate for wearables. Curvatures of forearms for different body types, especially children or infants with much smaller arms, needed to be considered. With a curvature, the resonant loop performance changed as the physical distributions of electromagnetic fields changed. Simulations were carried out by placing the resonator on curved arm models. Considering the shape of the sensing area in the forearm and various arm sizes, the curvature radius was estimated in a range of 45−190 mm to cover from infants to adults. The dehydrated and hydrated skin permittivity properties applied in the forearm model were measured by the dielectric probe (Keysight N1501 A) on the human body following the protocol mentioned before.

Fig. 17 shows the resonant frequencies for hydrated (red) and dehydrated skin (blue) in the selected curvature radius range from 45 to 190 mm. The circles indicate the calculated data. The resonant frequencies between hydrated and dehydrated states were distinguishable even with a small curvature radius. This is owing to the higher quality factor in resonance provided by the tuned loop resonator. The robust performance suggested that the sensor could be used in different body types.

B. ELECTRIC FIELD DISTRIBUTIONS

Human skin consists of three layers: epidermis, dermis, and hypodermis layers with typical mean thicknesses of 0.075, 1.3, and 8 mm on the inside of the forearm [70], [71], [72]. Measurement of skin impedance at low frequencies to evaluate hydration is limited by the current and field distributions that are mainly on the surface of the epidermis layer [73]. To effectively measure hydration levels in the body, higher frequency signals allow the fields to reach deeper into tissues. However, measuring reflection and transmission coefficients with transmitting and receiving antennas to probe tissue properties requires higher powers, and the penetration of RF energy through the body often raises safety concerns. The applications of a resonator on the skin to probe a local area potentially resolve the concerns. The dermis layer is typically 1.3 mm below the surface and contains blood vessels, including capillary loops and sweat glands [74]. Blood vessels directly carry water while sweat glands, controlled by the sympathetic nervous system, secrete water. The dermis layer also contains elastin and collagen fibers, as well as fat cells and fibroblasts, which respond slower to water changes compared to blood vessels and sweat glands [75]. Therefore, the field coverage needs to be sufficiently deep in order to include the effects of the blood vessel and sweat glands on the effective permittivity changes from water.

The tuned loop resonator is a near-field sensor since it is not effective for radiation with a tuning pad in the center. Simulations of field distributions were conducted. Fig. 18 shows

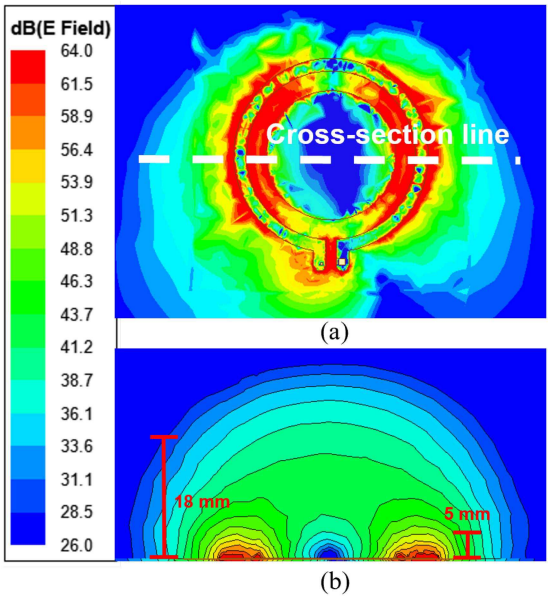

FIGURE 18. **Electric field distribution of the tuned loop. (a) The top view in the plane of the tuned loop. The side view is taken in the cross section (dashed line). (b) The side view into the tissues. The fields decay by 10 and 20 dB at depths of 5 and 18 mm.**

the top and side views of the electric fields at the resonant frequency of 900 MHz. The top view was taken in the plane of the tuned loop. The high electric fields were expected between the gap and around the outer ring. A standing wave was established for the tuned loop at the first resonance, so the fields had the lowest intensity between the gap in the middle of the loop, opposite to the port location. The side view revealed that the field magnitude decayed by 10 and 20 dB at depths of 5 and 18 mm, respectively, from the skin surface. The majority of the fields were confined in a cylinder with a diameter of 4 cm and a depth of 18 mm. Thus, we could assume the resonant frequencies were mainly determined by the effective permittivities in these specific areas. Given a sufficient field depth in the dermis and hypodermis layers to detect water influence in them, one does not need to worry about the energy penetrating too deep that it affects body functions or damages tissues.

VI. CONCLUSION

We have demonstrated a radio-frequency planar tuned loop resonator for non-invasive water content sensing within the body, potentially as a wearable on the forearm. Measurements and simulations were conducted to validate the feasibility. Discrepancies induced from the generalized tissue properties were verified. The high quality-factor of resonance in the tuned loop ensured the detection sensitivity for both the hydrated and dehydrated states. Utilizing measured effective permittivities in simulations verified the accuracy of using the planar resonator to detect hydration levels from a dehydrated state. Multiple experiments further demonstrated the feasibility of sensing hydration processes. A phantom was built to investigate the individuality of hydration levels in tissues and the resonance dependency on the tissue location. The dehydration experiments conducted with the phantoms showed the relative changes in resonant frequencies can be related to the water losses, and the dependency was due to the local permittivities. The shifting of resonant frequencies induced by the curvature of the forearm, taking into consideration of different body types, did not present an issue as the resonant frequencies were distinguishable between hydrated and dehydrated states. The field distributions were investigated by finite-element simulations showing the fields were confined with a limited area yet sufficiently deep to exploit the advantages of probing blood vessels and sweat glands in the dermis and hypodermis layers of skin. The localized sensing relieved the exposure safety concern from electromagnetic energy.

The multiple experiments on human bodies showed distinct and repeatable trends from the individual dehydrated states to fully hydrated ones. For individual persons, calibration at the fully hydrated state will be needed, and the resonance can track continuously if the person experiences dehydration, particularly in exercise or training activities, or for the elderly and children to monitor their water intake. With the advantages of being planar, compact, flexible, and with high sensitivity, the tuned loop resonator can be used as the sensing element in a wearable with comfort. The demonstrations with phantoms also show great potential for a variety of non-invasive water-sensing applications, for example, detecting water percentages of fruits in agriculture, probing tissues or organs as diagnostic tools, and monitoring water retention or absorption in the food processing industry.

REFERENCES

[1] S. N. Cheuvront and R. W. Kenefick, "Dehydration: Physiology, assessment, and performance effects," *Comprehensive Physiol.*, vol. 4, pp. 257–285, Jan. 2014.

[2] K. Watanabe, E. J. Stöhr, K. Akiyama, S. Watanabe, and J. GonzálezAlonso, "Dehydration reduces stroke volume and cardiac output during exercise because of impaired cardiac filling and venous return, not left ventricular function," *Physiol. Rep.*, vol. 8, no. 11, Jun. 2020, Art. no. e14433.

[3] J. C. Watso and W. B. Farquhar, "Hydration status and cardiovascular function," *Nutrients*, vol. 11, no. 8, Aug. 2019, Art. no. 1866.

[4] G. Arnaoutis et al., "The effect of hypohydration on endothelial function in young healthy adults," *Eur. J. Nutr.*, vol. 56, no. 3, pp. 1211–1217, Apr. 2017.

[5] N. I. Dmitrieva, D. Liu, and M. Boehm, "Increased risk of heart failure is associated with chronic habitual hypohydration that elevates serum sodium above 142 mmol/l suggesting lifelong optimal hydration as preventive measure," *Eur. Heart J.*, vol. 42, no. Supplement_1, Oct. 2021, Art. no. e053141.

[6] L. Jones, M. Cleary, R. Lopez, R. Zuri, and R. Lopez, "Active dehydration impairs upper and lower body anaerobic muscular power," *J. Strength Conditioning Res.*, vol. 22, no. 2, pp. 455–463, Mar. 2008.

[7] J. A. Kraft, J. M. Green, P. A. Bishop, M. T. Richardson, Y. H. Neggers, and J. D. Leeper, "The influence of hydration on anaerobic performance," *Res. Quart. Exercise Sport*, vol. 83, no. 2, pp. 282–292, Jun. 2012.

[8] I. Martínez-Navarro, A. Montoya-Vieco, E. Collado, B. Hernando, N. Panizo, and C. Hernando, "Muscle cramping in the marathon: Dehydration and electrolyte depletion vs. muscle damage," *J. Strength Conditioning Res.*, vol. 36, no. 6, pp. 1629–1635, Aug. 2020.

[9] J. D. Coso et al., "Muscle damage and its relationship with muscle fatigue during a half-iron triathlon," *PLoS ONE*, vol. 7, no. 8, 2012, Art. no. e43280.

[10] C. Roncal-Jimenez, M. A. Lanaspa, T. Jensen, L. G. Sanchez-Lozada, and R. J. Johnson, "Mechanisms by which dehydration may lead to chronic kidney disease," *Ann. Nutr. Metab.*, vol. 66, no. 3, pp. 10–13, Jan. 2015.

[11] G. Strippoli, J. Craig, E. Rochtchina, V. Flood, J. Wang, and P. Mitchell, "Fluid and nutrient intake and risk of chronic kidney disease," *Nephrology*, vol. 16, no. 3, pp. 326–334, Mar. 2011.

[12] J. M. Sontrop et al., "Association between water intake, chronic kidney disease, and cardiovascular disease: A cross-sectional analysis of NHANES data," *Amer. J. Nephrol.*, vol. 37, no. 5, pp. 434–442, May 2013.

[13] C. Bongers et al., "Impact of acute versus prolonged exercise and dehydration on kidney function and injury," *Physiol. Rep.*, vol. 6, no. 11, 2018, Art. no. e13734.

[14] C. L. Chapman, B. D. Johnson, N. T. Vargas, D. Hostler, M. D. Parker, and Z. J. Schlader, "Both hyperthermia and dehydration during physical work in the heat contribute to the risk of acute kidney injury," *J. Appl. Physiol.*, vol. 128, no. 4, pp. 715–728, Apr. 2020.

[15] J. A. Lo et al., "Impact of water consumption on renal function in the general population: A cross-sectional analysis of KNHANES data (2008–2017)," *Clin. Exp. Nephrol.*, vol. 25, no. 4, pp. 376–384, Jan. 2021.

[16] D. H. Wegman et al., "Intervention to diminish dehydration and kidney damage among sugarcane workers," *Scand. J. Work, Environ. Health*, vol. 44, no. 1, pp. 16–24, Jan. 2018.

[17] M. C. Houser et al., "Inflammation-related factors identified as biomarkers of dehydration and subsequent acute kidney injury in agricultural workers," *Biol. Res. Nurs.*, vol. 23, no. 4, pp. 676–688, Oct. 2021.

[18] S. Ninan, C. Walton, and G. Barlow, "Investigation of suspected urinary tract infection in older people," *BMJ. Brit. Med. J.*, vol. 349, no. 7972, p. g4070, Aug. 2014.

[19] M. Ramzan, S. Bakhsh, A. Salam, G. M. Khan, and G. Mustafa, "Risk factors in urinary tract infection," *Gomal J. Med. Sci.*, vol. 2, no. 1, pp. 11–21, Jun. 2004.

[20] F. Manz and A. Wentz, "The importance of good hydration for the prevention of chronic diseases," *Nutr. Rev.*, vol. 63, no. Supplement_1, pp. 2–5, Jun. 2005.

[21] I. McQuarrie, "Epilepsy in children: The relationship of water balance to the occurrence of seizures," *Amer. J. Dis. Child.*, vol. 38, no. 3, pp. 451–467, Sep. 1929.

[22] R. D. Andrew, "Seizure and acute osmotic change: Clinical and neurophysiological aspects," *J. Neurological Sci.*, vol. 101, no. 1, pp. 7–18, 1991.

[23] R. D. Andrew, M. Fagan, B. A. Ballyk, and A. S. Rosen, "Seizure susceptibility and the osmotic state," *Brain Res.*, vol. 498, no. 1, pp. 175–180, 1989.

[24] A. K. Doumbia et al., "Seizures in children under five in a pediatric ward: Prevalence, associated factors and outcomes," *Open J. Pediatrics*, vol. 11, no. 4, pp. 627–635, 2021.

[25] N. A. Masento, M. Golightly, D. T. Field, L. T. Butler, and C. M. van Reekum, "Effects of hydration status on cognitive performance and mood," *Brit. J. Nutr.*, vol. 111, no. 10, pp. 1841–1852, May 2014.

[26] J. M. Dickson et al., "The effects of dehydration on brain volume - preliminary results," *Int. J. Sports Med.*, vol. 26, no. 6, pp. 481–485, 2005.

[27] M. Lauriola et al., "Neurocognitive disorders and dehydration in older patients: Clinical experience supports the hydromolecular hypothesis of dementia," *Nutrients*, vol. 10, no. 5, May 2018, Art. no. 562.

[28] W. F. Clark et al., "Urine volume and change in estimated GFR in a community-based cohort study," *Clin. J. Amer. Soc. Nephrol.*, vol. 6, no. 11, pp. 2634–2641, Nov. 2011.

[29] B. M. Popkin, K. E. D'Anci, and I. H. Rosenberg, "Water, hydration, and health," *Nutr. Rev.*, vol. 68, no. 8, pp. 439–458, Aug. 2010.

[30] K. E. D'Anci, F. Constant, and I. H. Rosenberg, "Hydration and cognitive function in children," *Nutr. Rev.*, vol. 64, no. 10, pp. 457–464, Oct. 2006.

[31] M. H. Gorelick, K. N. Shaw, and K. O. Murphy, "Validity and reliability of clinical signs in the diagnosis of dehydration in children," *Pediatrics*, vol. 99, no. 5, p. e6, May 1997.

[32] P. A. Phillips et al., "Reduced thirst after water deprivation in healthy elderly men," *New England J. Med.*, vol. 311, no. 12, pp. 753–759, Sep. 1984.

[33] N. S. Stachenfeld, C. A. Leone, E. S. Mitchell, E. Freese, and L. Harkness, "Water intake reverses dehydration associated impaired executive function in healthy young women," *Physiol. Behav.*, vol. 185, pp. 103–111, Mar. 2018.

[34] R. F. Reinoso, B. A. Telfer, and M. Rowland, "Tissue water content in rats measured by desiccation," *J. Pharmacological Toxicological Methods*, vol. 38, no. 2, pp. 87–92, 1997.

[35] H. P. Schwan and K. R. Foster, "Microwave dielectric properties of tissue. Some comments on the rotational mobility of tissue water," *Biophys. J.*, vol. 17, no. 2, pp. 193–197, 1977.

[36] S. D. Meo et al., "The variability of dielectric permittivity of biological tissues with water content," *J. Electromagn. Waves Appl.*, vol. 36, no. 1, pp. 48–68, Jan. 2022.

[37] A. Shahzad, S. Khan, M. Jones, R. M. Dwyer, and M. O'Halloran, "Investigation of the effect of dehydration on tissue dielectric properties in EX vivo measurements," *Biomed. Phys. Eng. Exp.*, vol. 3, no. 4, Jun.26, 2017, Art. no. 45001.

[38] D. A. Pollacco, L. Farina, P. S. Wismayer, L. Farrugia, and C. V. Sammut, "Characterization of the dielectric properties of biological tissues and their correlation to tissue hydration," *IEEE Trans. Dielectrics. Elect. Insul.*, vol. 25, no. 6, pp. 2191–2197, Dec. 2018.

[39] R. Balduino et al., "Feasibility of water content-based dielectric characterization of biological tissues using mixture models," *IEEE Trans. Dielectrics. Elect. Insul.*, vol. 26, no. 1, pp. 187–193, Feb. 2019.

[40] A. Shahzad, A. Elahi, P. Donlon, and M. O'Halloran, "A water dependent tissue dielectric model for estimation of in-vivo dielectric properties," in *Proc. IEEE MTT-S Int. Microw. Biomed. Conf.*, 2020, pp. 1–3.

[41] G. Maenhout, A. Santorelli, E. Porter, I. Ocket, T. Markovic, and B. Nauwelaers, "Effect of dehydration on dielectric measurements of biological tissue as function of time," *IEEE J. Electromagn. RF Microw. Med. Biol.*, vol. 4, no. 3, pp. 200–207, Sep. 2020.

[42] A. Peyman, A. A. Rezazadeh, and C. Gabriel, "Changes in the dielectric properties of rat tissue as a function of age at microwave frequencies," *Phys. Med. Biol.*, vol. 46, no. 6, pp. 1617–1629, Jun. 2001.

[43] E. Nyfors, "Industrial microwave sensors-A review," *Sens. Imag.*, vol. 1, no. 1, pp. 23–43, Jan. 2000.

[44] G. S. Raghavan and M. S. Venkatesh, "An overview of dielectric properties measuring techniques," *Can. Biosyst. Eng.*, vol. 47, no. 7, pp. 15–30, Jan. 2005.

[45] M. P. Robinson, J. Clegg, and D. A. Stone, "A novel method of studying total body water content using a resonant cavity: Experiments and numerical simulation," *Phys. Med. Biol.*, vol. 48, no. 1, pp. 113–125, Jan. 2003.

[46] D. A. Stone and M. P. Robinsons, "Total body water content observations using cavity - perturbation techniques," in *Proc. High Freq. Postgraduate Student Colloq.*, 2003, pp. 31–34.

[47] A. W. Kraszewski, S. O. Nelson, and T. S. You, "Use of a microwave cavity for sensing dielectric properties of arbitrarily shaped biological objects," *IEEE Trans. Microw. Theory Techn.*, vol. 38, no. 7, pp. 858–863, Jul. 1990.

[48] H. Choi et al., "Design and in vitro interference test of microwave noninvasive blood glucose monitoring sensor," *IEEE Trans. Microw. Theory Techn.*, vol. 63, no. 10, pp. 3016–3025, Oct. 2015.

[49] H. Choi, S. Luzio, J. Beutler, and A. Porch, "Microwave noninvasive blood glucose monitoring sensor: Human clinical trial results," in *Proc. IEEE MTT-S Int. Microw. Symp.*, Honolulu, HI, USA, 2017, pp. 876–879.

[50] M. Baghelani, Z. Abbasi, M. Daneshmand, and P. E. Light, "Non-invasive continuous-time glucose monitoring system using a chipless printable sensor based on split ring microwave resonators," *Sci. Rep.*, vol. 10, no. 1, 2020, Art. no. 12980.

[51] M. Puentes, M. Maasch, M. Schussler, and R. Jakoby, "Frequency multiplexed 2-dimensional sensor array based on split-ring resonators for organic tissue analysis," *IEEE Trans. Microw. Theory Techn.*, vol. 60, no. 6, pp. 1720–1727, Jun. 2012.

[52] S. Hardinata, F. Deshours, G. Alquie, H. Kokabi, and F. Koskas, "Complementary split-ring resonators for non-invasive characterization of biological tissues," in *Proc. 18th Int. Symp. Antenna Technol. Appl. Electromagn.*, 2018, pp. 1–2.

[53] D. C. Garrett and E. C. Fear, "Feasibility study of hydration monitoring using microwaves-Part 1: A model of microwave property changes with dehydration," *IEEE J. Electromagn. RF Microw. Med. Biol.*, vol. 3, no. 4, pp. 292–299, Dec. 2019.

[54] D. C. Garrett, J. R. Fletcher, D. B. Hogan, T. S. Fung, and E. C. Fear, "Feasibility study of hydration monitoring using microwaves-Part 2: Measurements of athletes," *IEEE J. Electromagn. RF Microw. Med. Biol.*, vol. 3, no. 4, pp. 300–307, Dec. 2019.
[55] B. C. Besler and E. C. Fear, "Microwave hydration monitoring: System assessment using fasting volunteers," *MDPI Sensors*, vol. 21, no. 21, Oct.20, 2021, Art. no. 6949.
[56] R. Brendtke, M. Wiehl, F. Groeber, T. Schwarz, H. Walles, and J. Hansmann, "Feasibility study on a microwave-based sensor for measuring hydration level using human skin models," *PLoS One*, vol. 11, no. 4, Apr. 2016, Art. no. e0153145.
[57] J. Kilpijärvi, J. Tolvanen, J. Juuti, N. Halonen, and J. Hannu, "A non-invasive method for hydration status measurement with a microwave sensor using skin phantoms," *IEEE Sensors J.*, vol. 20, no. 2, pp. 1095–1104, Jan. 2020.
[58] A. F. McKinley, T. P. White, I. S. Maksymov, and K. R. Catchpole, "The analytical basis for the resonances and anti-resonances of loop antennas and meta-material ring resonators," *J. Appl. Phys.*, vol. 112, no. 9, Nov. 2012, Art. no. 94911.
[59] J. Wei, "Distributed capacitance of planar electrodes in optic and acoustic surface wave devices," *IEEE J. Quantum Electron.*, vol. 13, no. 4, pp. 152–158, Apr. 1977.
[60] F. Maradei and S. Caniggia, "Appendix A: Formulae for partial inductance calculation," in *Signal Integrity and Radiated Emission of High-Speed Digital Systems.* Chichester, U.K.: Wiley, 2008, pp. 481–486.
[61] S. Bing, K. Chawang, and J.-C. Chiao, "A resonant coupler for subcutaneous implant," *MDPI Sensors*, vol. 21, no. 23, Dec. 2021, Art. no. 8141.
[62] S. Bing, K. Chawang, and J. C. Chiao, "Resonant coupler designs for subcutaneous implants," in *Proc. IEEE Wireless Power Transfer Conf.*, 2021, pp. 1–4.
[63] D. Andreuccetti, R. Fossi, and C. Petrucci, "An internet resource for the calculation of the dielectric properties of body tissues in the frequency range 10 Hz-100 GHz," 1997. [Online]. Available: http://niremf.ifac.cnr.it/tissprop/
[64] G. Maenhout, T. Markovic, I. Ocket, and B. Nauwelaers, "Effect of open-ended coaxial probe-to-tissue contact pressure on dielectric measurements," *MDPI Sensors*, vol. 20, no. 7, Apr. 2020, Art. no. 2060.
[65] A. H. Sihvola and J. A. Kong, "Effective permittivity of dielectric mixtures," *IEEE Trans. Geosci. Remote Sens.*, vol. 26, no. 4, pp. 420–429, Jul. 1988.
[66] S. Evans, "Dielectric properties of ice and snow-a review," *J. Glaciology*, vol. 5, no. 42, pp. 773–792, 1965.
[67] K. Sasaki, E. Porter, E. A. Rashed, L. Farrugia, and G. Schmid, "Measurement and image-based estimation of dielectric properties of biological tissues-past, present, and future," *Phys. Med. Biol.*, vol. 67, no. 14, Jul. 2022, Art. no. 14TR01.
[68] S. Gabriel, R. W. Lau, and C. Gabriel, "The dielectric properties of biological tissues: III parametric models for the dielectric spectrum of tissues," *Phys. Med. Biol.*, vol. 41, no. 11, pp. 2271–2293, Nov. 1996.
[69] J. G. Lyng, L. Zhang, and N. P. Brunton, "A survey of the dielectric properties of meats and ingredients used in meat product manufacture," *Meat Sci.*, vol. 69, no. 4, pp. 589–602, 2005.
[70] W. F. W. Southwood, "The thickness of the skin," *Plast. Reconstructive Surg.*, vol. 15, no. 5, pp. 423–429, May 1955.
[71] Y. Lee and K. Hwang, "Skin thickness of korean adults," *Surg. Radiologic Anatomy*, vol. 24, no. 3/4, pp. 183–189, 2002.
[72] J. Sandby-Møller, T. Poulsen, and H. Wulf, "Epidermal thickness at different body sites: Relationship to age, gender, pigmentation, blood content, skin type and smoking habits," *Acta Dermato-Venereologica*, vol. 83, no. 6, pp. 410–413, Nov. 2003.
[73] X. Huang et al., "Epidermal impedance sensing sheets for precision hydration assessment and spatial mapping," *IEEE Trans. Biomed. Eng.*, vol. 60, no. 10, pp. 2848–2857, Oct. 2013.
[74] F. M. Hendriks, D. Brokken, C. W. J. Oomens, D. L. Bader, and F. P. T. Baaijens, "The relative contributions of different skin layers to the mechanical behavior of human skin in vivo using suction experiments," *Med. Eng. Phys.*, vol. 28, no. 3, pp. 259–266, 2006.
[75] Y. Feldman et al., "The electromagnetic response of human skin in the millimetre and submillimetre wave range," *Phys. Med. Biol.*, vol. 54, no. 11, pp. 3341–3363, Jun. 2009.

SEN BING (Graduate Student Member, IEEE) received the Bachelor of Technology degree in electronics and information science and technology from Hainan Normal University, Haikou, China, in 2013, and the Master of Science degree in electrical engineering from Southern Methodist University, Dallas, TX, USA, in 2019. He is currently working toward the Ph.D. degree in electrical and computer engineering with Southern Methodist University. He has authored/co-authored one journal paper and seven conference papers on optimizing performance for microwave biomedical sensor and implant, four conference papers on factors affecting pH performance and one conference paper on low-cost ultrasound medical imaging. His research interests on microwave biomedical devices, electro-chemical biosensors, wearable electronics, medical imaging, and RF devices.

KHENGDAULIU CHAWANG (Student Member, IEEE) received the Bachelor of Technology degree in electronics and communication engineering from National Institute of Technology, India, in 2012, and the Master of Science degree in electrical engineering from the University of Texas, Arlington, TX, USA, in 2019. She is currently working toward the Ph.D. degree in electrical and computer engineering with Southern Methodist University, Dallas, TX, USA. She has authored/co-authored seven conference papers on factors affecting pH performance. Her research focuses on flexible and ultra-flexible devices by micro and nano fabrication, electro-chemical biosensors, wearable electronics, and RF devices.

J.-C. CHIAO (Fellow, IEEE) received the B.S. degree from the Electrical Engineering Department, National Taiwan University, New Taipei, Taiwan, in 1988, and the M.S. and Ph.D. degrees in electrical engineering from the California Institute of Technology, Pasadena, CA, USA, in 1991 and 1995, respectively. He was a Research Scientist with Optical Networking Systems and Testbeds Group, Bell Communications Research, Assistant Professor of electrical engineering with the University of Hawaii, Manoa, Honolulu, HI, USA, and Product Line Manager and Senior Technology Advisor with Chorum Technologies. He was Janet and Mike Greene endowed Professor and Jenkins Garrett Professor of electrical engineering with the University of Texas – Arlington, TX, USA, from 2002 to 2018. He is currently Mary and Richard Templeton Centennial Chair Professor of electrical and computer engineering with Southern Methodist University (SMU), Dallas, TX, USA. He has been the Chair and Technical Program Chair of several international conferences including 2018 IEEE International Microwave Biomedical Conference and 2021 IEEE Wireless Power Transfer Conference. He was the Chair for the IEEE MTT-S Technical Committee ten Biological Effect and Medical Applications of RF and Microwave, and Associate Editor for IEEE TRANSACTIONS ON MICROWAVE THEORY AND TECHNIQUES. He was the founding Editor-in-Chief of IEEE JOURNAL OF ELECTROMAGNETICS, RF, AND MICROWAVES IN MEDICINE AND BIOLOGY. He is on the Editorial Board of IEEE ACCESS and Track Editor of IEEE JOURNAL OF MICROWAVES. He has authored or coauthored and edited numerous peer-reviewed technical journal and conference papers, book chapters, proceedings and books. He holds 20 patents in RF MEMS, MEMS optical, liquid crystal, nano-scale fabrication, and wireless medical sensor technologies. His research works have been covered by media extensively including *Forbes, National Geographic* magazine, National Public Radio and CBS Henry Ford Innovation Nation. Dr. Chiao was the recipient of Lockheed Martin Aeronautics Company Excellence in Engineering Teaching Award, Tech. Titans Technology Innovator Award, Research in Medicine award in the Heroes of Healthcare, IEEE Region five Outstanding Engineering Educator award; IEEE Region five Excellent Performance Award, 2012−2014 IEEE MTT Distinguished Microwave Lecturer, 2017−2019 IEEE Sensors Council Distinguished Lecturer, Pan Wen-Yuan Foundation Excellence in Research Award, and the 2011 Edith and Peter O'Donnell Award in Engineering by The Academy of Medicine, Engineering and Science of Texas. Dr. Chiao is a Fellow of IET, SPIE and AIMBE.